

000
 001
 002
 003
004 Supplementary Material to “External Prior Guided Internal Prior Learning for
 005 **Real Noisy Image Denoising”**

006
 007
 008 Anonymous CVPR submission
 009
 010
 011 Paper ID 1047
 012
 013
 014 In this supplementary material, we provide:
 015 1. The closed-form solution of the sparse coding problem (6) in the main paper.
 016 2. More denoising results on the real noisy images in dataset [1].
 017 3. More results on the 15 cropped real noisy images (with mean image of 500 shots as “ground truth”) in dataset [2].
 018 4. More results on the 60 cropped real noisy images (with mean image of 500 shots as “ground truth”) in dataset [2].
 019
 020 **021 1. Closed-Form Solution of the Weighted Sparse Coding Problem (6)**
 022
 023 For notation simplicity, we ignore the indices n, m, t in problem (6) of the main paper. It turns into the following weighted
 024 sparse coding problem:
 025
$$\min_{\alpha} \|\mathbf{y} - \mathbf{D}\alpha\|_2^2 + \sum_{j=1}^{3p^2} \lambda_j |\alpha_j|. \quad (1)$$

026 Since \mathbf{D} is an orthogonal matrix, problem (1) is equivalent to
 027
 028
$$\min_{\alpha} \|\mathbf{D}^T \mathbf{y} - \alpha\|_2^2 + \sum_{j=1}^{3p^2} \lambda_j |\alpha_j|. \quad (2)$$

031 For simplicity, we denote $\mathbf{z} = \mathbf{D}^T \mathbf{y}$. Here we have $\lambda_j > 0, j = 1, \dots, 3p^2$, then problem (2) can be written as:
 032
 033
$$\min_{\alpha} \sum_{j=1}^{3p^2} ((\mathbf{z}_j - \alpha_j)^2 + \lambda_j |\alpha_j|). \quad (3)$$

035 The problem (3) is separable w.r.t. each α_j and hence can be simplified to $3p^2$ independent scalar minimization problems
 036
 037
$$\min_{\alpha_j} (\mathbf{z}_j - \alpha_j)^2 + \lambda_j |\alpha_j|, \quad (4)$$

038 where $j = 1, \dots, 3p^2$. Taking derivative of α_j in problem (4) and setting the derivative to be zero. There are two cases for the
 039 solution.
 040

041 (a) If $\alpha_j \geq 0$, we have
 042

$$2(\alpha_j - \mathbf{z}_j) + \lambda_j = 0. \quad (5)$$

043 The solution is
 044

$$\hat{\alpha}_j = \mathbf{z}_j - \frac{\lambda_j}{2} \geq 0. \quad (6)$$

045 So $\mathbf{z}_j \geq \frac{\lambda_j}{2} > 0$, and the solution $\hat{\alpha}_j$ can be written as
 046

$$\hat{\alpha}_j = \text{sgn}(\mathbf{z}_j) * (|\mathbf{z}_j| - \frac{\lambda_j}{2}), \quad (7)$$

049 where $\text{sgn}(\bullet)$ is the sign function.
 050

051 (b) If $\alpha_j < 0$, we have
 052

$$2(\alpha_j - \mathbf{z}_j) - \lambda_j = 0. \quad (8)$$

053 The solution is
 054

$$\hat{\alpha}_j = \mathbf{z}_j + \frac{\lambda_j}{2} < 0. \quad (9)$$

108 So $\mathbf{z}_j < -\frac{\lambda_j}{2} < 0$, and the solution $\hat{\alpha}_j$ can be written as
 109

$$\hat{\alpha}_j = \text{sgn}(\mathbf{z}_j) * (-\mathbf{z}_j - \frac{\lambda_j}{2}) = \text{sgn}(\mathbf{z}_j) * (|\mathbf{z}_j| - \frac{\lambda_j}{2}). \quad (10)$$

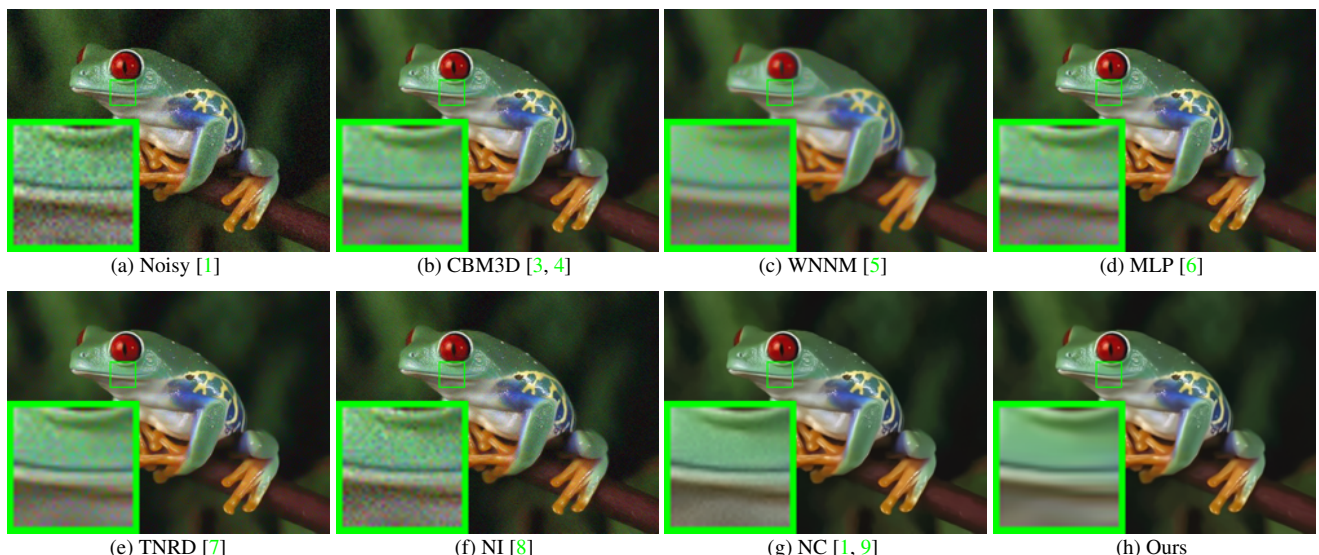
110 In summary, we have the final solution of the weighted sparse coding problem (1) as
 111

$$\hat{\alpha} = \text{sgn}(\mathbf{D}^T \mathbf{y}) \odot \max(|\mathbf{D}^T \mathbf{y}| - \lambda, 0), \quad (11)$$

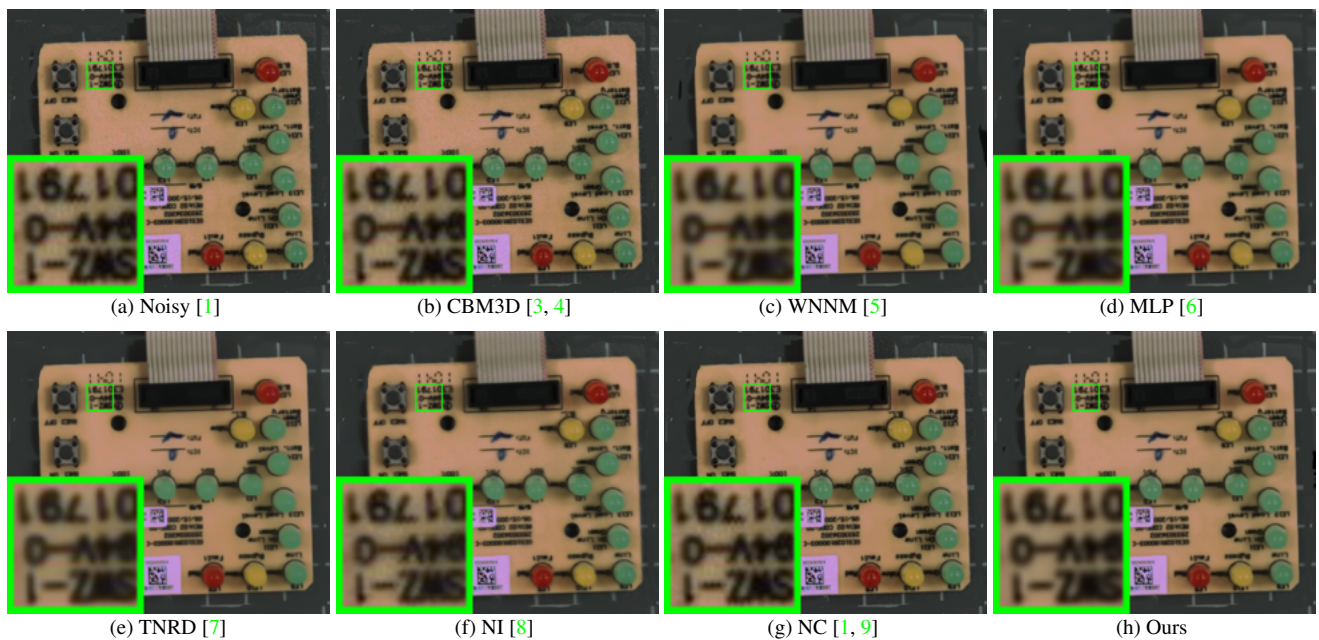
112 where $\lambda = \frac{1}{2}[\lambda_1, \lambda_2, \dots, \lambda_{3p^2}]^\top$ is the vector of regularization parameter and \odot means element-wise multiplication.
 113

114 2. More Denoising Results on the Real Noisy Images in Dataset [1]

115 In this section, we give more comparisons of the competing methods on the dataset [1]. The real noisy images in dataset
 116 [1] have no “ground truth” images and hence we only compare the visual quality of the denoised images by different methods.
 117 As can be seen from Figures 1-4, our proposed method performs better than the state-of-the-art denoising methods.
 118



119 Figure 1. Denoised images of the real noisy image “Frog” [1] by different methods. The images are better to be zoomed in on screen.
 120



121 Figure 2. Denoised images of the real noisy image “Circuit” [1] by different methods. The images are better to be zoomed in on screen.
 122

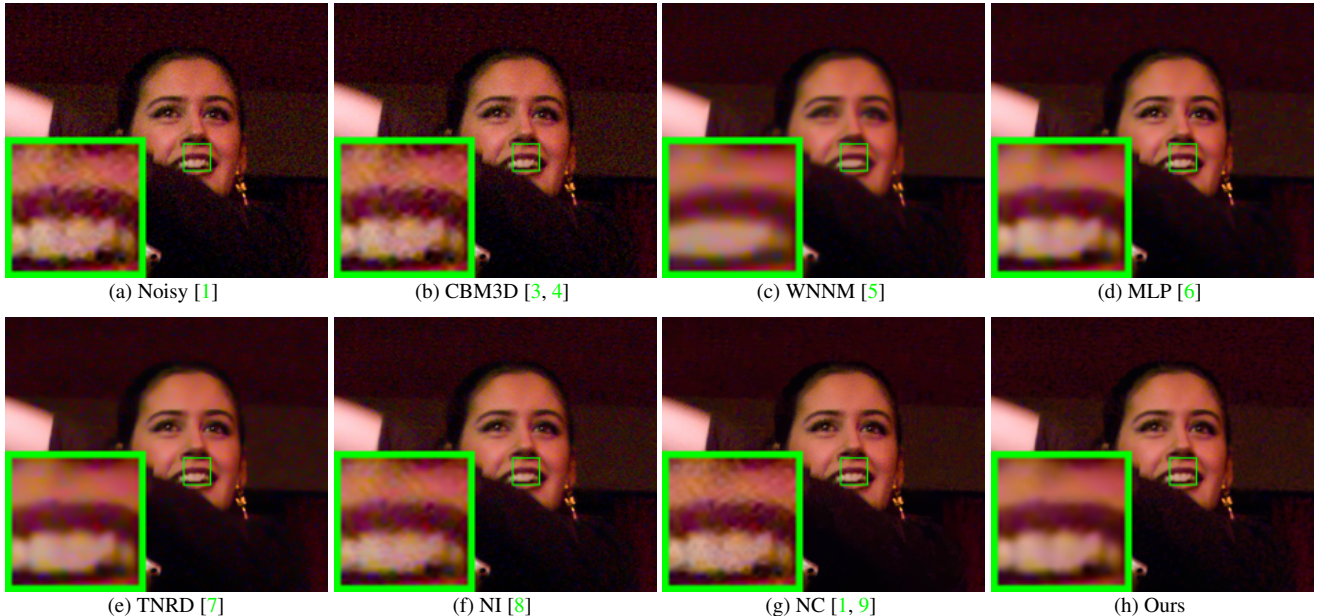
216
217
218
219
220
221
222
223
224
225
226

Figure 3. Denoised images of the real noisy image “Woman” [1] by different methods. The images are better to be zoomed in on screen.

236

237

238

239

240

241

242

243

244

245

246

247

248

249

250

251

252

253

254

255

256

257

258

259

260

261

262

263

264

265

266

267

268

269

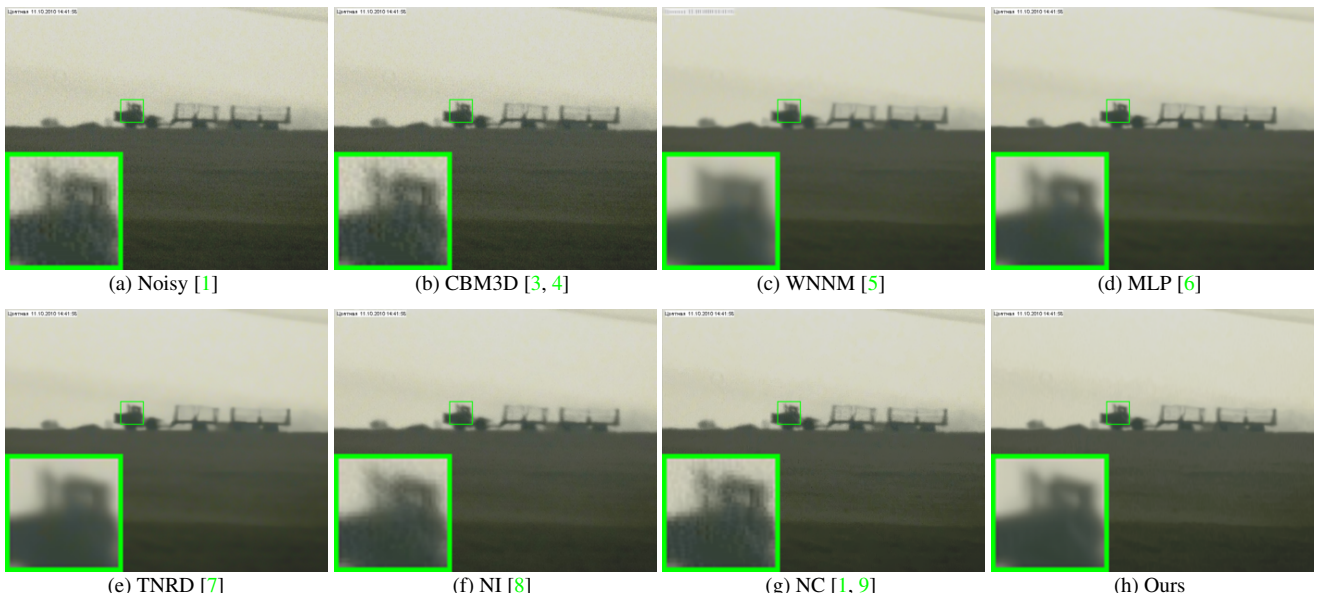
270
271
272
273
274
275
276
277
278
279
280
281
282
283
284
285
286
287
288
289
290
291
292
293
294
295
296
297
298
299
300
301
302
303
304
305
306
307
308
309
310
311
312
313
314
315
316
317
318
319
320
321
322
323

Figure 4. Denoised images of the real noisy image “Vehicle” [1] by different methods. The images are better to be zoomed in on screen.

3. More Denoising Results on the 15 Cropped Images Used in [2]

In this section, we provide more visual comparisons of the proposed method with the state-of-the-art denoising methods on the 15 cropped real noisy images used in [2]. In this dataset, each scene was shot 500 times under the same camera and camera setting. The mean image of the 500 shots is roughly taken as the “ground truth”, with which the PSNR can be computed. As can be seen from Figures 5-9, in most cases, our proposed method achieves better performance than the competing methods. This validates the effectiveness of our proposed external prior guided internal prior learning framework for real noisy image denoising.

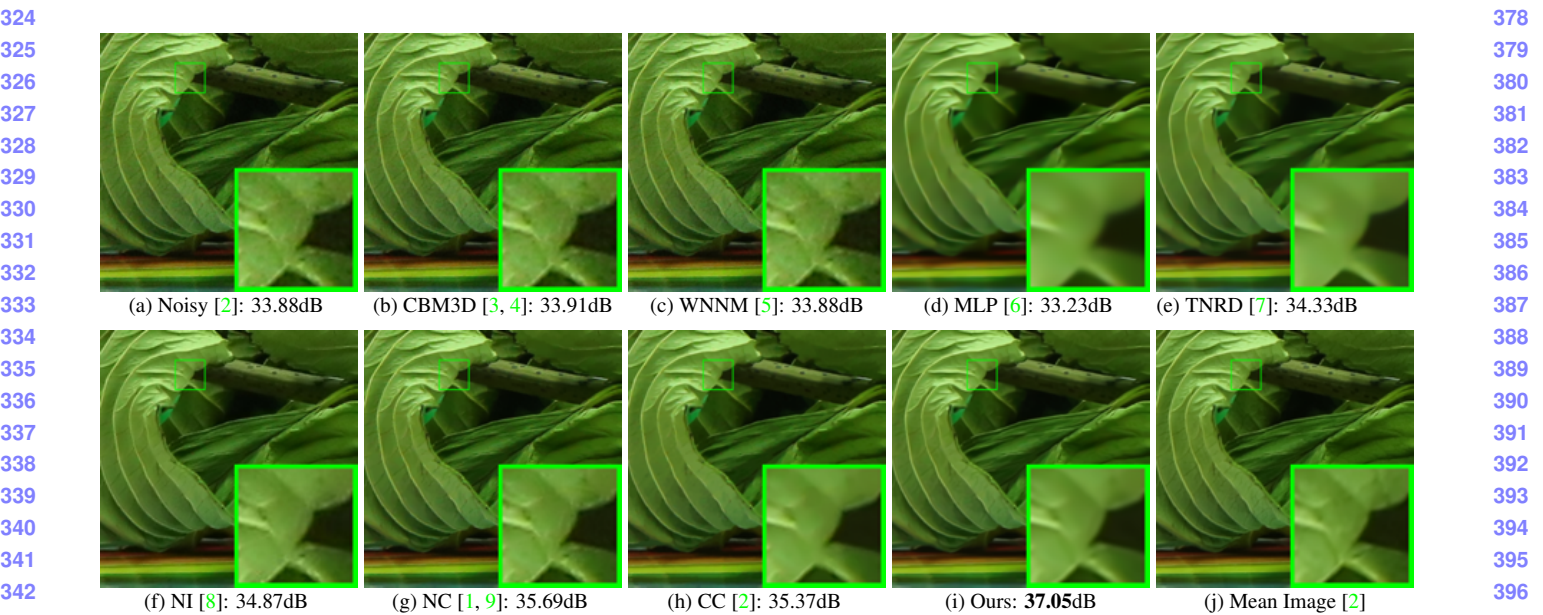


Figure 5. Denoised images of a region cropped from the real noisy image “Canon 5D Mark 3 ISO 3200 2” [2] by different methods. The images are better to be zoomed in on screen.

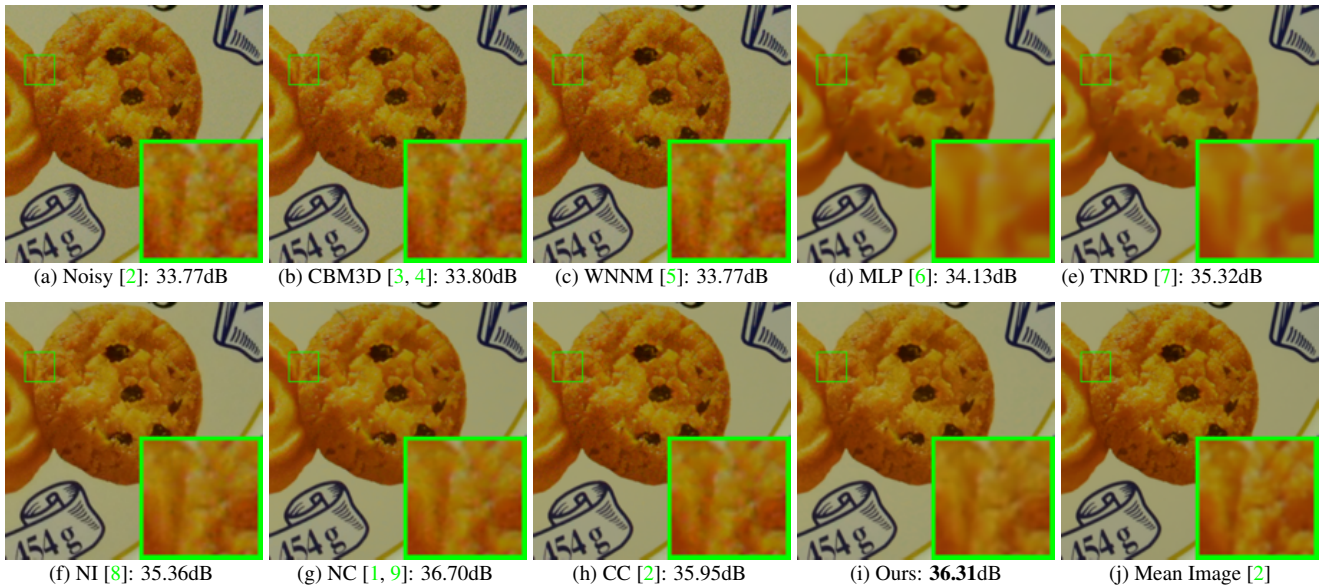


Figure 6. Denoised images of a region cropped from the real noisy image “Nikon D600 ISO 3200 2” [2] by different methods. The images are better to be zoomed in on screen.

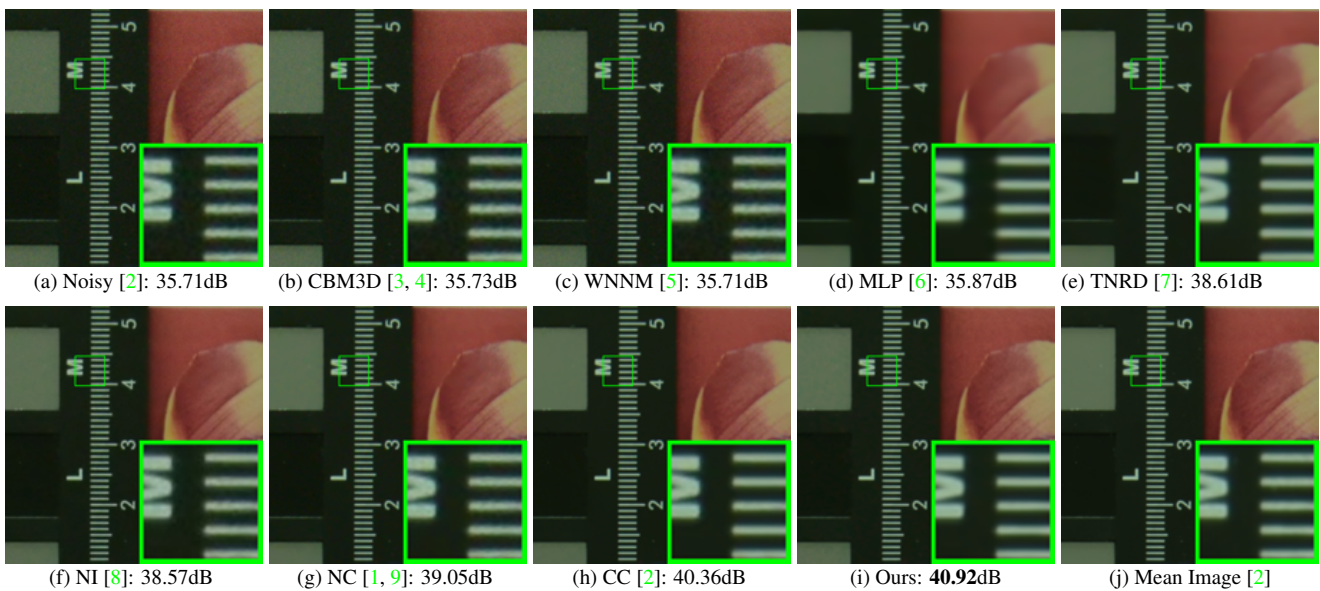


Figure 7. Denoised images of a region cropped from the real noisy image “Nikon D800 ISO 1600 2” [2] by different methods. The images are better to be zoomed in on screen.

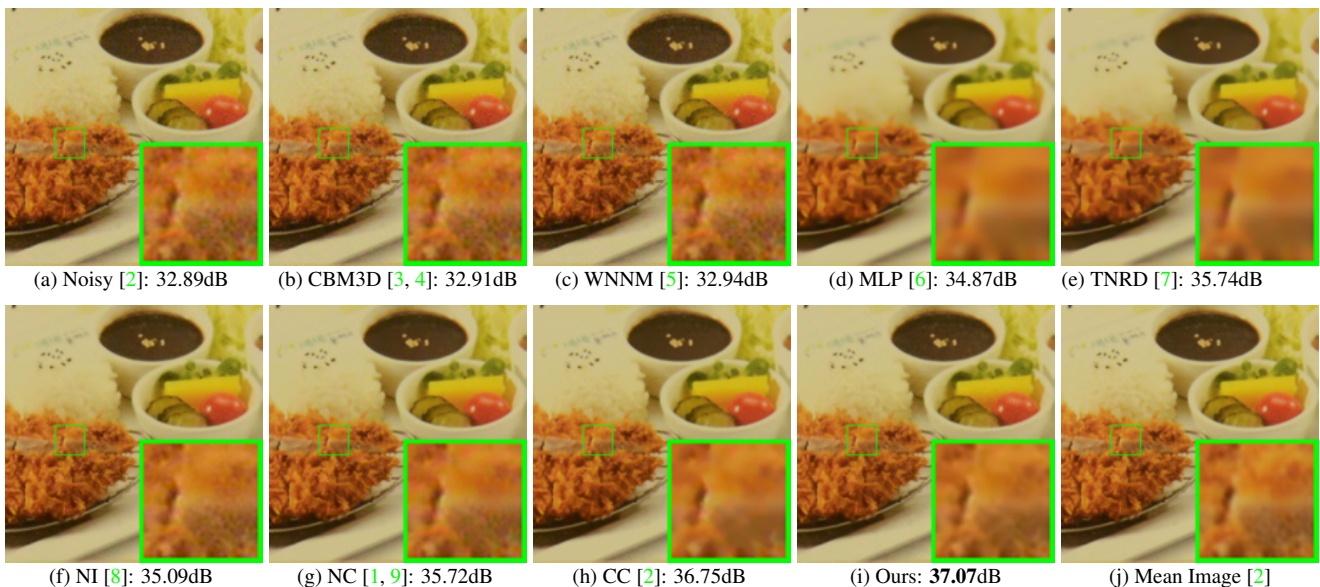


Figure 8. Denoised images of a region cropped from the real noisy image “Nikon D800 ISO 3200 2” [2] by different methods. The images are better to be zoomed in on screen.

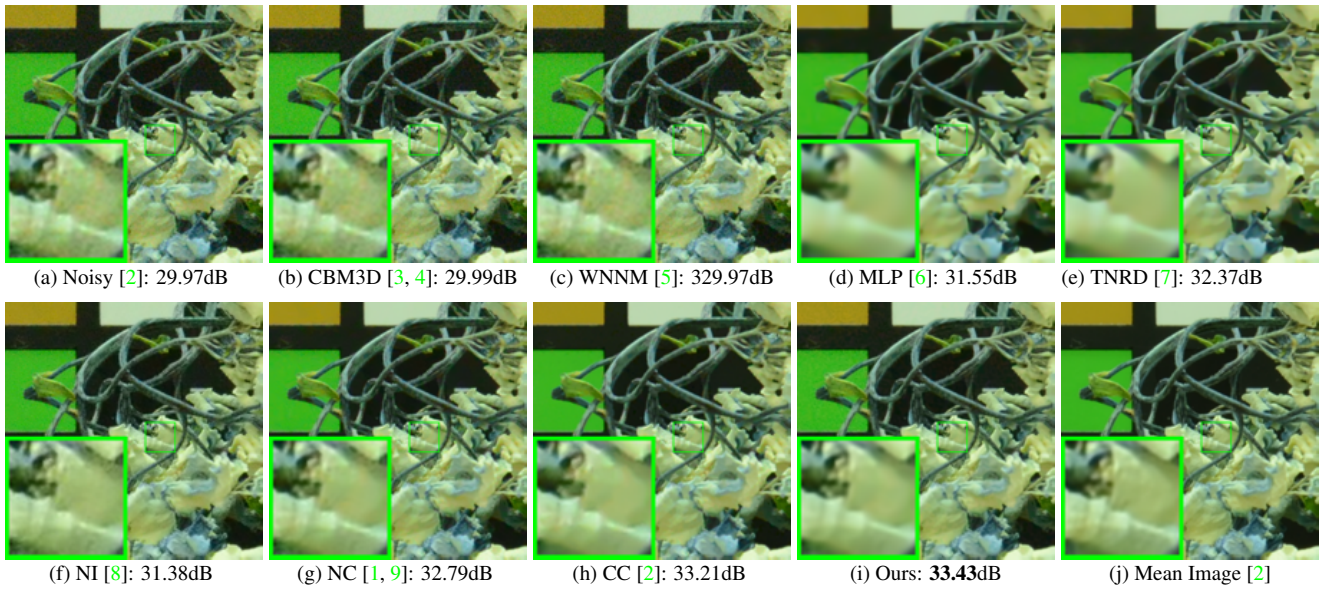


Figure 9. Denoised images of a region cropped from the real noisy image “Nikon D800 ISO 6400 2” [2] by different methods. The images are better to be zoomed in on screen.

4. More Denoising Results on the 60 Cropped Real Noisy Images from [2]

In this section, we provide more visual comparisons of the proposed method with the state-of-the-art denoising methods on the 60 cropped real noisy images we cropped from [2]. In this dataset, each scene was shot 500 times under the same camera and camera setting. The mean image of the 500 shots is roughly taken as the “ground truth”, with which the PSNR can be computed. As can be seen from Figures 10-20, in most cases, our proposed method achieves better performance than the competing methods. This validates the effectiveness of our proposed external prior guided internal prior learning framework for real noisy image denoising.

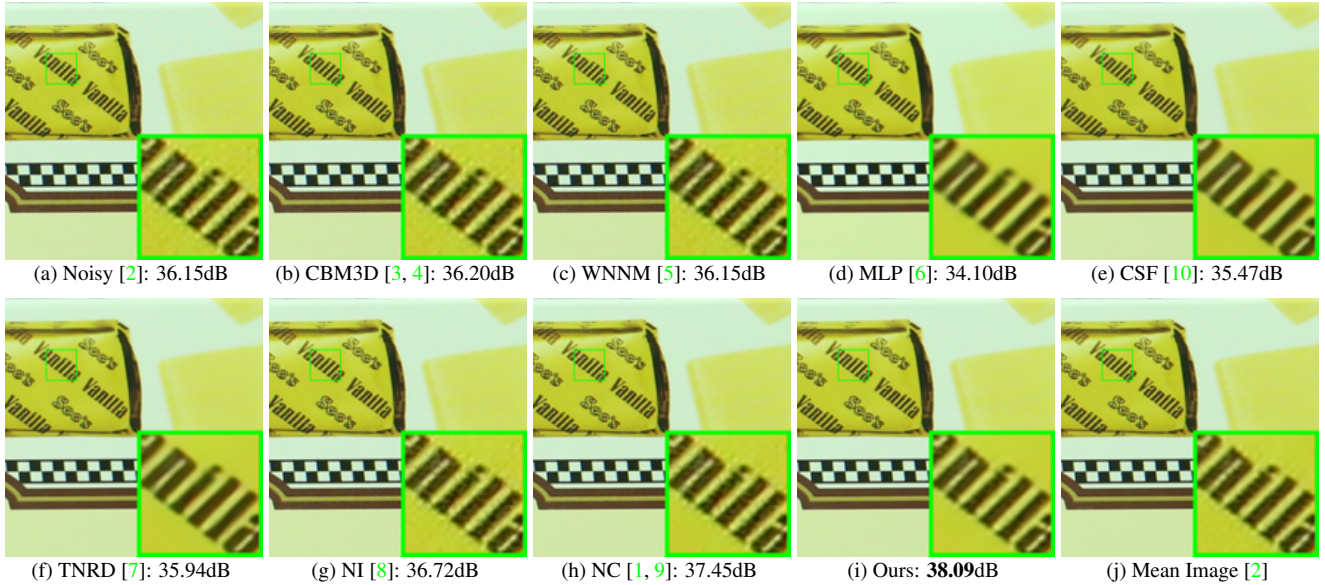


Figure 10. Denoised images of a region cropped from the real noisy image “Canon EOS 5D Mark3 ISO 3200 C1” [2] by different methods. The images are better viewed by zooming in on screen.

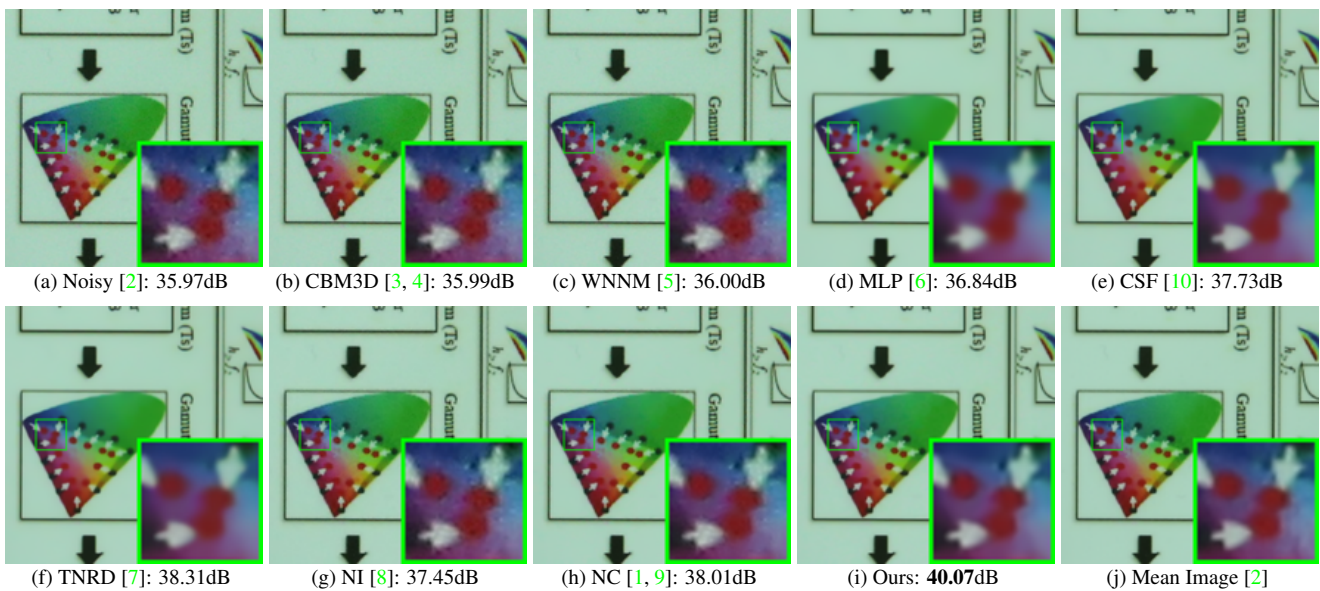


Figure 11. Denoised images of a region cropped from the real noisy image “Canon EOS 5D Mark3 ISO 3200 C2” [2] by different methods. The images are better viewed by zooming in on screen.

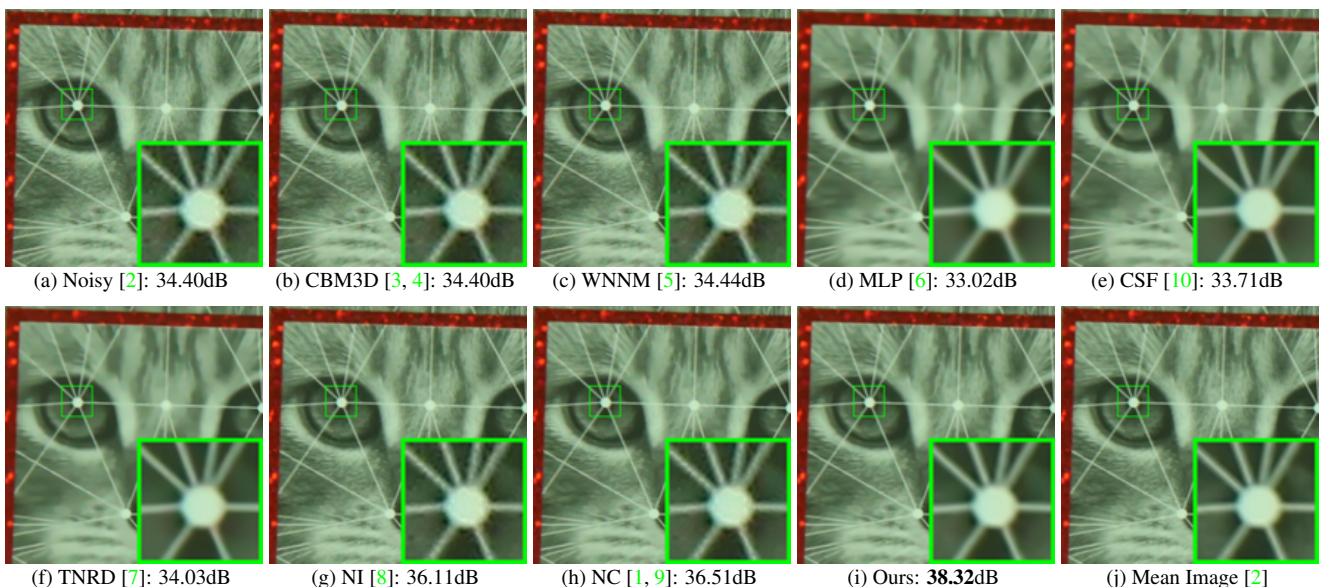


Figure 12. Denoised images of a region cropped from the real noisy image “Canon EOS 5D Mark3 ISO 3200 C3” [2] by different methods. The images are better viewed by zooming in on screen.

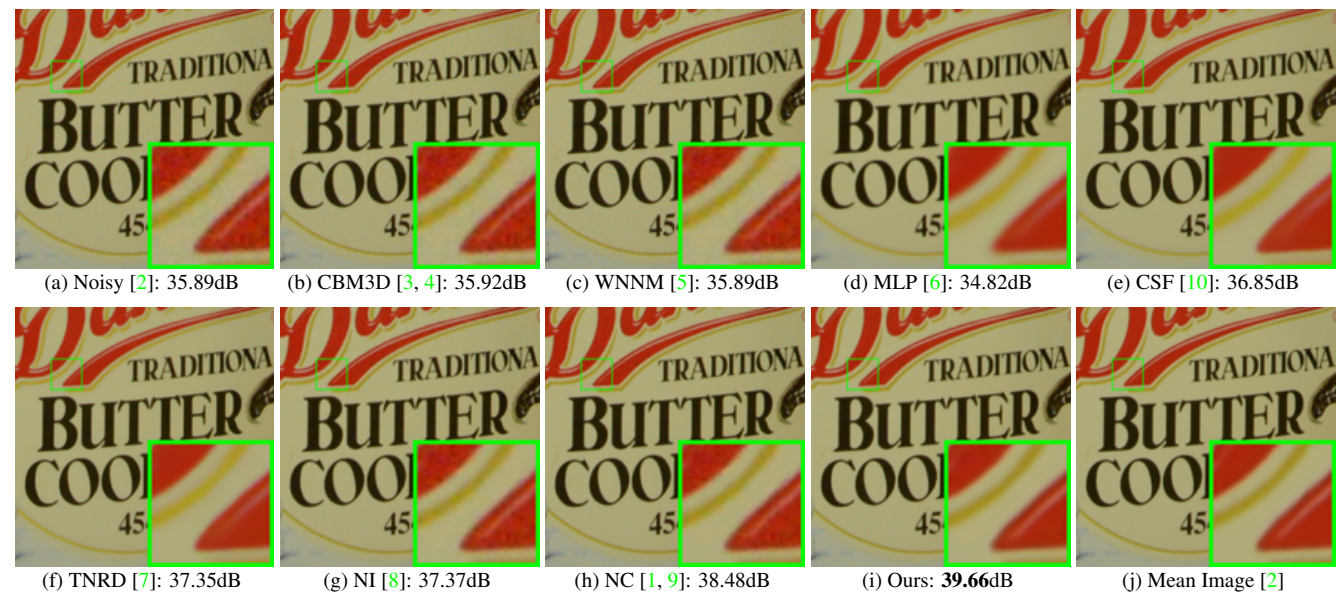


Figure 13. Denoised images of a region cropped from the real noisy image “Nikon D600 ISO 3200 C1” [2] by different methods. The images are better viewed by zooming in on screen.

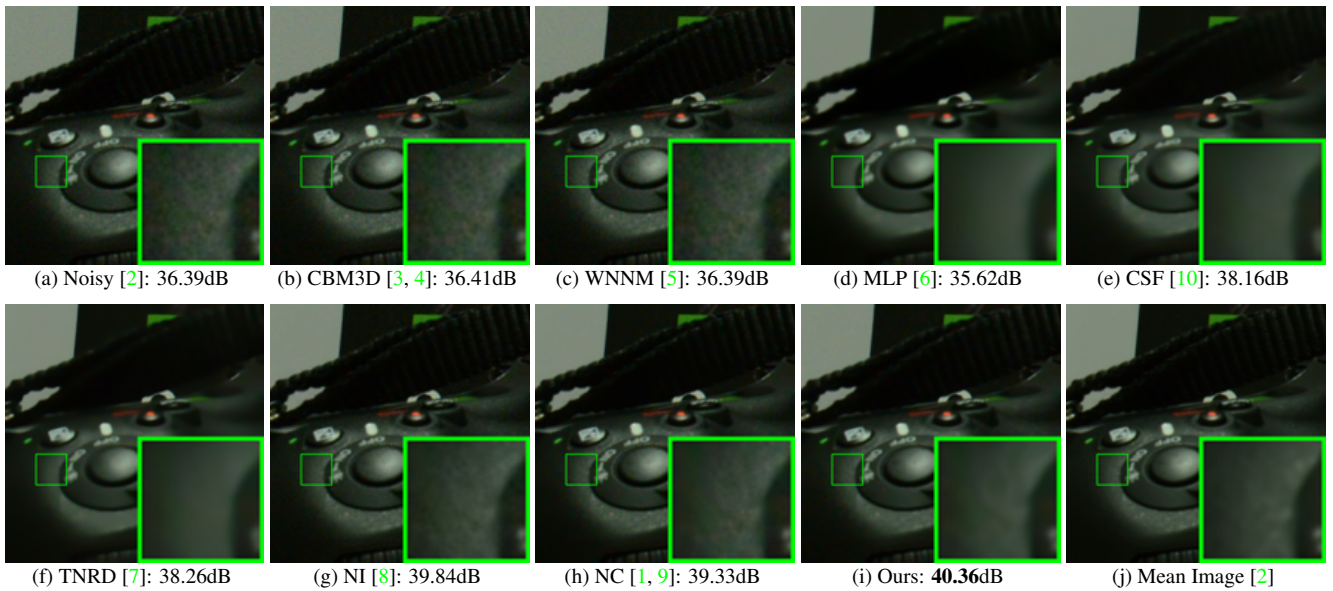


Figure 14. Denoised images of a region cropped from the real noisy image “Nikon D600 ISO 3200 C2” [2] by different methods. The images are better viewed by zooming in on screen.

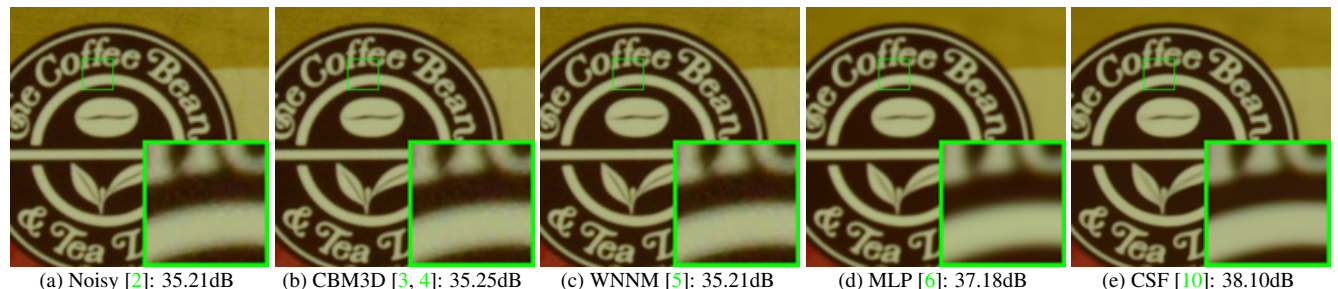


Figure 15. Denoised images of a region cropped from the real noisy image “Nikon D800 ISO 1600 B2” [2] by different methods. The images are better viewed by zooming in on screen.

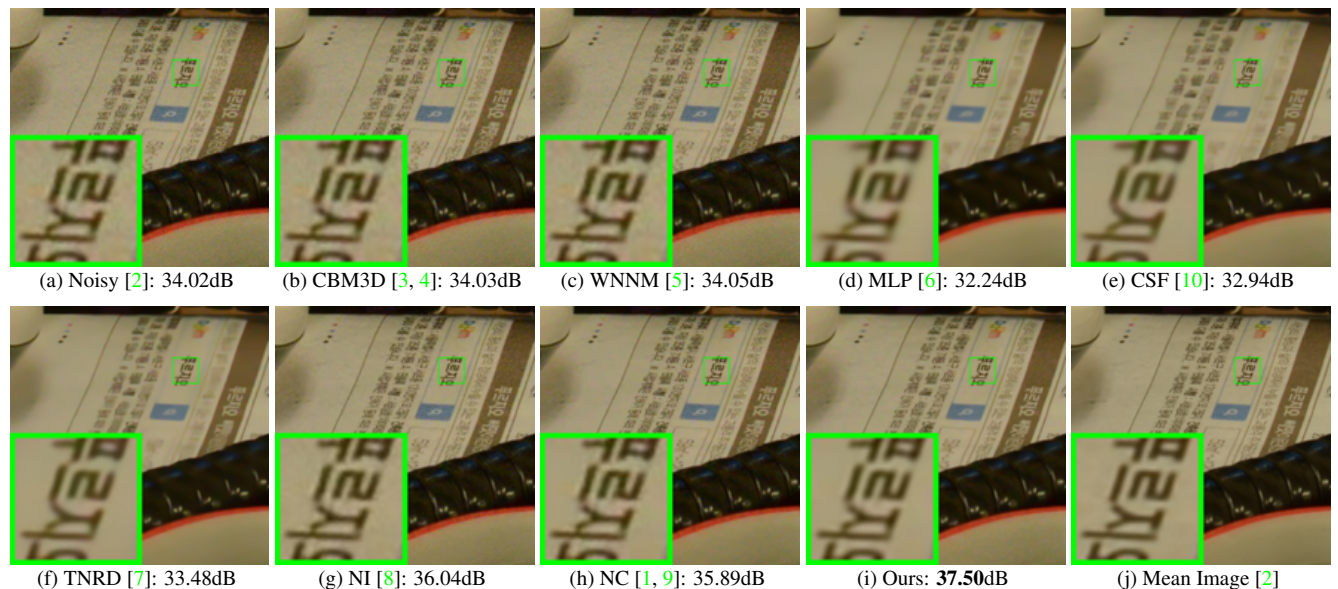


Figure 16. Denoised images of a region cropped from the real noisy image “Nikon D800 ISO 3200 A1” [2] by different methods. The images are better viewed by zooming in on screen.

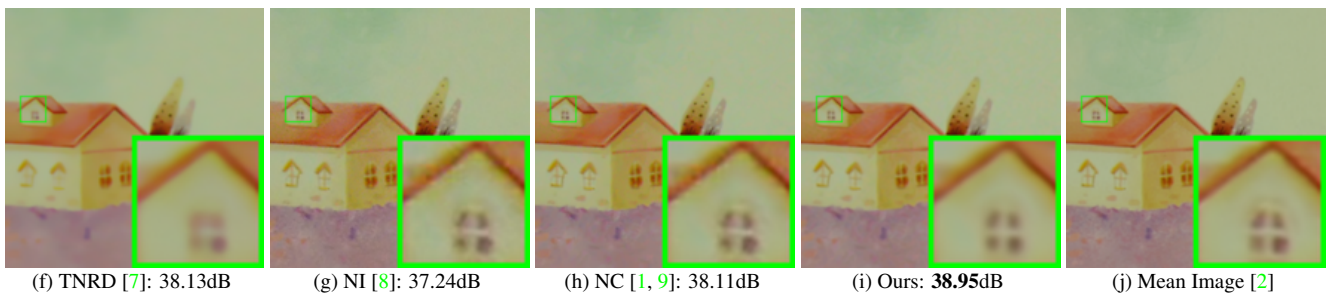
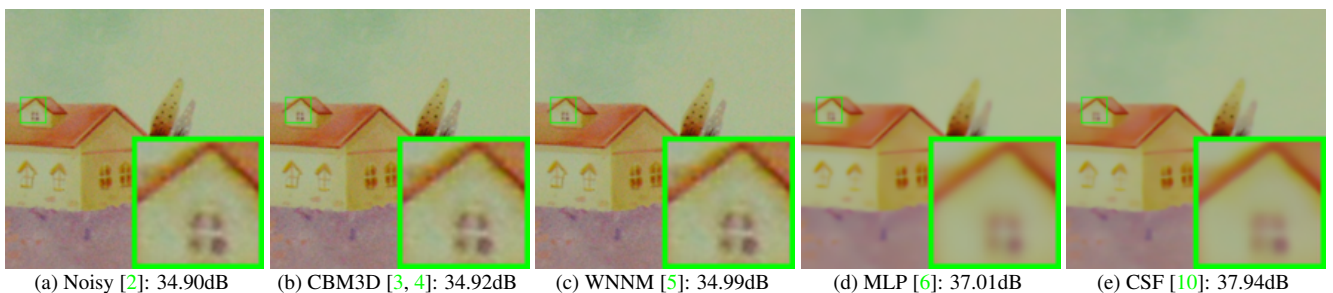


Figure 17. Denoised images of a region cropped from the real noisy image “Nikon D800 ISO 3200 A2” [2] by different methods. The images are better viewed by zooming in on screen.

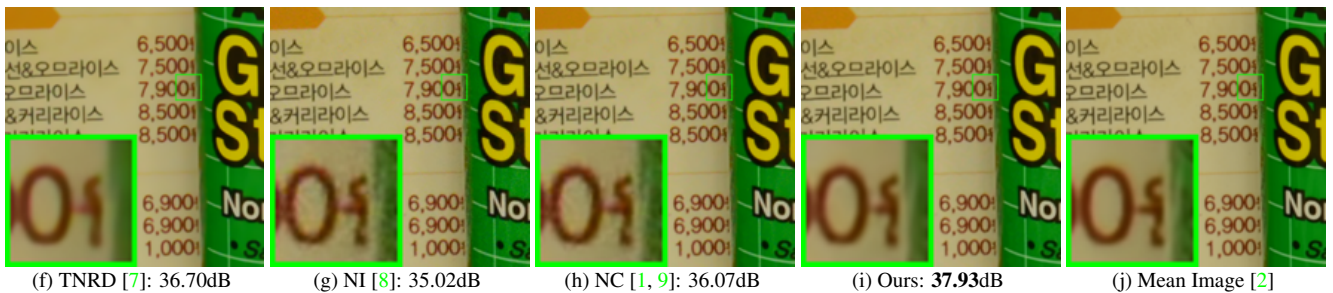
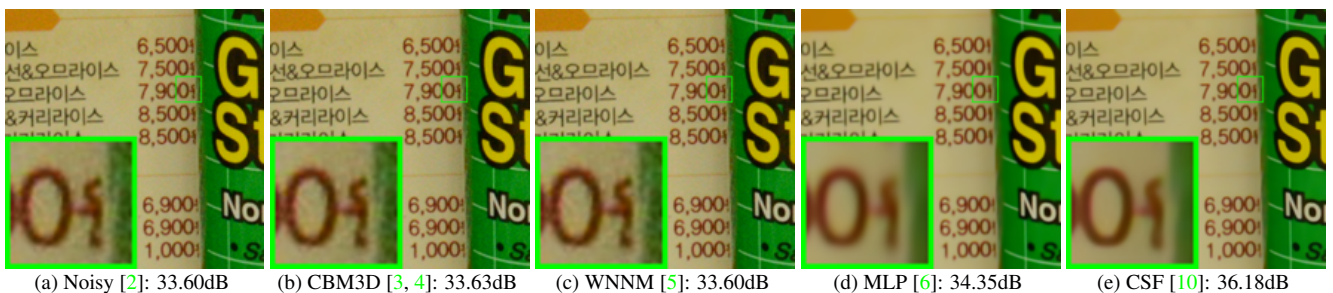


Figure 18. Denoised images of a region cropped from the real noisy image “Nikon D800 ISO 3200 A3” [2] by different methods. The images are better viewed by zooming in on screen.

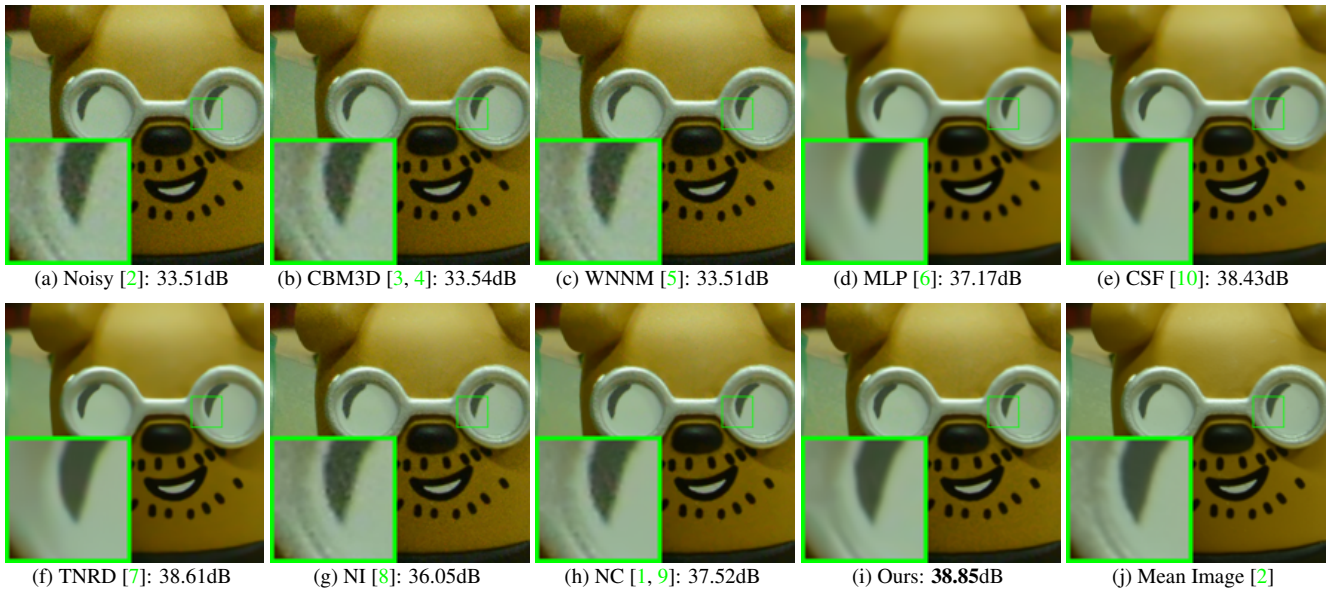


Figure 19. Denoised images of a region cropped from the real noisy image “Nikon D800 ISO 3200 A4” [2] by different methods. The images are better viewed by zooming in on screen.

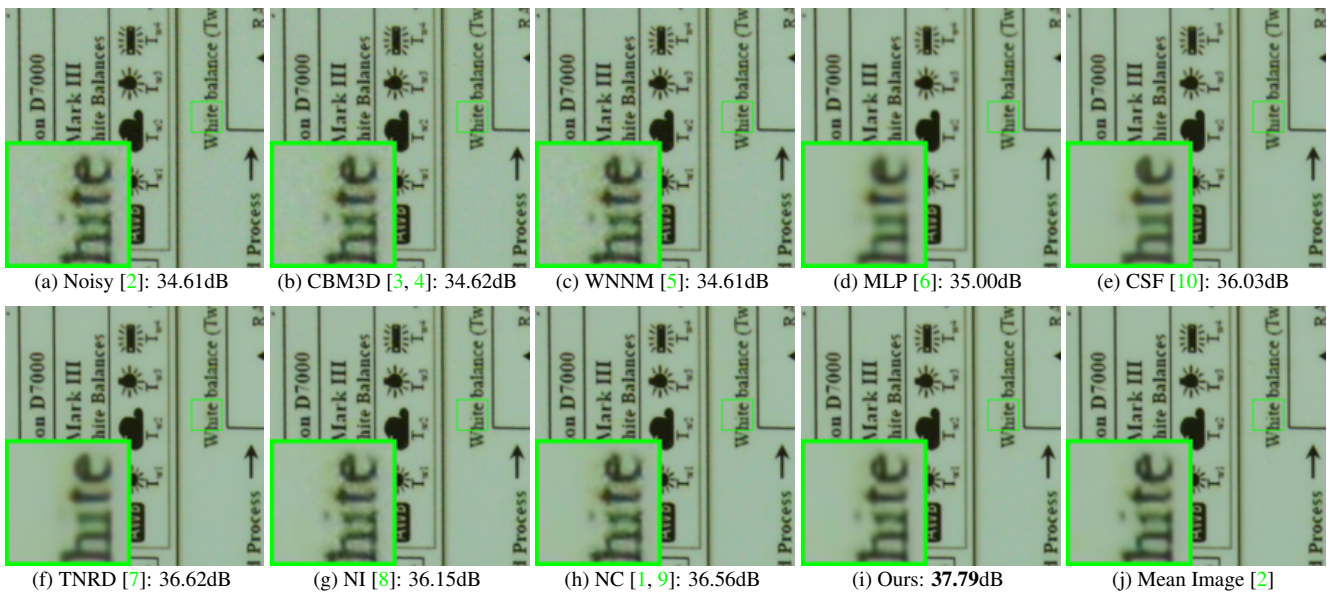


Figure 20. Denoised images of a region cropped from the real noisy image “Nikon D800 ISO 3200 A5” [2] by different methods. The images are better viewed by zooming in on screen.

References

- [1] M. Lebrun, M. Colom, and J. M. Morel. The noise clinic: a blind image denoising algorithm. <http://www.ipol.im/pub/art/2015/125/>. Accessed 01 28, 2015. 1, 2, 3, 4, 5, 6, 7, 8, 9, 10, 11
- [2] S. Nam, Y. Hwang, Y. Matsushita, and S. J. Kim. A holistic approach to cross-channel image noise modeling and its application to image denoising. *IEEE Conference on Computer Vision and Pattern Recognition (CVPR)*, pages 1683–1691, 2016. 1, 3, 4, 5, 6, 7, 8, 9, 10, 11
- [3] K. Dabov, A. Foi, V. Katkovnik, and K. Egiazarian. Image denoising by sparse 3-D transform-domain collaborative filtering. *IEEE Transactions on Image Processing*, 16(8):2080–2095, 2007. 2, 3, 4, 5, 6, 7, 8, 9, 10, 11

- 1188 [4] K. Dabov, A. Foi, V. Katkovnik, and K. Egiazarian. Color image denoising via sparse 3D collaborative filtering with grouping
1189 constraint in luminance-chrominance space. *IEEE International Conference on Image Processing (ICIP)*, pages 313–316, 2007. 2, 1242
1190 3, 4, 5, 6, 7, 8, 9, 10, 11 1243
1191 [5] S. Gu, L. Zhang, W. Zuo, and X. Feng. Weighted nuclear norm minimization with application to image denoising. *IEEE Conference*
1192 *on Computer Vision and Pattern Recognition (CVPR)*, pages 2862–2869, 2014. 2, 3, 4, 5, 6, 7, 8, 9, 10, 11 1244
1193 [6] H. C. Burger, C. J. Schuler, and S. Harmeling. Image denoising: Can plain neural networks compete with BM3D? *IEEE Conference*
1194 *on Computer Vision and Pattern Recognition (CVPR)*, pages 2392–2399, 2012. 2, 3, 4, 5, 6, 7, 8, 9, 10, 11 1245
1195 [7] Y. Chen, W. Yu, and T. Pock. On learning optimized reaction diffusion processes for effective image restoration. *IEEE Conference*
1196 *on Computer Vision and Pattern Recognition (CVPR)*, pages 5261–5269, 2015. 2, 3, 4, 5, 6, 7, 8, 9, 10, 11 1246
1197 [8] Neatlab ABSoft. Neat Image. <https://ni.neatvideo.com/home>. 2, 3, 4, 5, 6, 7, 8, 9, 10, 11 1247
1198 [9] M. Lebrun, M. Colom, and J.-M. Morel. Multiscale image blind denoising. *IEEE Transactions on Image Processing*, 24(10):3149–
1200 3161, 2015. 2, 3, 4, 5, 6, 7, 8, 9, 10, 11 1248
1201 [10] U. Schmidt and S. Roth. Shrinkage fields for effective image restoration. *IEEE Conference on Computer Vision and Pattern Recog-*
1202 *nition (CVPR)*, pages 2774–2781, June 2014. 6, 7, 8, 9, 10, 11 1249
1203
1204
1205
1206
1207
1208
1209
1210
1211
1212
1213
1214
1215
1216
1217
1218
1219
1220
1221
1222
1223
1224
1225
1226
1227
1228
1229
1230
1231
1232
1233
1234
1235
1236
1237
1238
1239
1240
1241